

Submitted to The Astrophysical Journal Letters on 28/2/2005

The first giant flare from SGR 1806–20: observations with the INTEGRAL SPI Anti-Coincidence Shield

S. Mereghetti, D. Götz

*Istituto di Astrofisica Spaziale e Fisica Cosmica,
Sezione di Milano "G.Occhialini" - INAF
v.Bassini 15, I-20133 Milano, Italy
sandro@mi.iasf.cnr.it*

A. von Kienlin, A. Rau, G. Lichten

*Max-Planck-Institut für extraterrestrische Physik, Giessenbachstrasse,
Postfach 1312, D-85741 Garching, Germany*

G. Weidenspointner, P. Jean

*Centre d'Étude Spatiale des Rayonnements
31028 Toulouse, France*

ABSTRACT

A giant flare from the Soft Gamma-ray Repeater SGR 1806–20 has been detected by several satellites on 2004 December 27. This tremendous outburst, the first one observed from this source, was a hundred times more powerful than the two previous giant flares from SGR 0525–66 and SGR 1900+14. We report the results obtained for this event with the Anticoincidence Shield of the SPI spectrometer on board the INTEGRAL satellite, which provides a high-statistics light curve at $E \gtrsim 80$ keV. The initial short peak, which saturated the detector for ~ 0.7 s, was followed by a ~ 400 s long tail modulated at the neutron star rotation period of 7.56 s. The tail fluence corresponds to an energy in photons above 3 keV of $1.6 \times 10^{44} d_{15kpc}^2$ erg. This is of the same order of the energy emitted in the pulsating tails of the two giant flares seen from other soft repeaters, despite the hundredfold larger overall emitted energy of the SGR 1806–20 giant flare. Long lasting (~ 1 hour) hard X-ray emission, decaying in time as $\sim t^{-0.85}$, and likely associated to the SGR 1806–20 giant flare afterglow has also been detected.

Subject headings:

1. Introduction

Soft Gamma-ray Repeaters (SGRs) are high-energy sources characterized by sporadic periods of activity in which they emit short bursts (<1 s) with energy up to $\sim 10^{41}$ erg. They are believed to be highly magnetized ($B \sim 10^{14}$ – 10^{15} G) neutron stars, or "magnetars" (see Woods & Thompson 2004 for a recent review). Large soft γ -ray flares, reaching peak luminosities above several 10^{44} erg s $^{-1}$ and lasting a few minutes, have been observed from two SGRs: on 1979 March 5 from SGR 0525–66 (Mazets et al. 1979) and on 1998 August 27 from SGR 1900+14 (Hurley et al. 1999; Feroci et al. 1999). The detection of only two of such giant outbursts from different sources in about 30 years implies that these events, involving energy releases of more than 10^{44} ergs, are relatively rare.

SGR 1806–20 is currently the most prolific of the four known SGRs. Its level of activity has been increasing in the last few years, during which many bursts have been detected with different satellites, including RXTE (Göğüş et al. 2001; Ibrahim et al. 2003; Woods et al. 2004) and INTEGRAL (Götz et al. 2004). On 2004 October 5 two clusters of strong bursts with a total fluence of $\sim 10^{-4}$ erg cm $^{-2}$ were emitted within a time span of a few minutes (Mereghetti et al. 2004). It was noted (Golenetskii et al. 2004a) that a similar event occurred in SGR 1900+14 three months before its 1998 giant outburst (Aptekar et al. 2001). The increasing level of activity in SGR 1806–20 was also reflected in the properties of its quiescent X-ray emission. XMM-Newton observations showed that its 2–10 keV luminosity doubled and the spectrum became harder in 2004 (Mereghetti et al. 2005b). A similar trend was present in the persistent 20–150 keV emission discovered with INTEGRAL observations carried out in 2003–2004 (Mereghetti et al. 2005a).

The energetic activity of SGR 1806–20 culminated on 2004 December 27, when more than twenty satellites recorded the first giant outburst from this source. The hard X-ray flux during the initial pulse was so large to saturate most detectors (Borkowski et al. 2004; Hurley et al. 2004; Mazets et al. 2004; Golenetskii et al. 2004b; Palmer et al. 2004; Smith et al. 2005; Boggs et al. 2005) and to significantly ionize the Earth's upper atmosphere (Campbell et al. 2005). Here we report the properties of this giant outburst derived with the Anticoincidence Shield (ACS) of the SPI spectrometer on board the INTEGRAL satellite.

2. The SPI Anti-Coincidence Shield

The Anti-Coincidence Shield (ACS) of SPI consists of 91 BGO scintillator crystals of thickness between 16 and 50 mm and with a total mass of 512 kg. Besides serving as a veto for the SPI germanium spectrometer, the ACS is able to detect gamma-ray bursts from a

large fraction of the sky (von Kienlin et al. 2003). The data used here consist of the overall ACS count rate (i.e. the read out from the sum of the 91 crystals) sampled in time intervals of 50 ms. No energy or directional information is available. The ACS is sensitive to photons above a low-energy threshold corresponding to approximately 80 keV. However, due to the different properties of the various BGO blocks, their associated photomultipliers, and the chosen redundancy concept (the signals from two different crystals are fed to the same FEE), this threshold is not sharp and its exact value not well determined.

Dead time and saturation effects in the crystals and electronics are negligible (<1%) for total count rates smaller than a few 10^5 cts s $^{-1}$. When this condition is verified we can easily convert the observed count rates to an incident energy flux, assuming a spectral shape and knowing the ACS effective area. The latter is a function of the incidence angle, with a maximum for directions nearly orthogonal to the satellite pointing axis and unobstructed by other instruments. At the time of the flare SGR 1806–20 was at a zenith angle $\theta=106^\circ$ from the SPI pointing axis and at an azimuth angle $\phi=9^\circ$ ($\phi=0^\circ$ corresponds to the satellite Sun-pointing side, i.e. the direction from SPI toward the IBIS instrument). The ACS effective area as a function of energy for this direction has been computed by means of Monte Carlo simulations based on detailed mass modelling (Weidenspointner et al. 2003 and references therein) of the SPI spectrometer and of the surrounding material (satellite structure and other instruments). The effective area increases monotonically with energy; it is about 340 cm 2 at 100 keV, about 1150 cm 2 at 200 keV, and larger than 3000 cm 2 above 1 MeV. Thus the ACS provides the data with the best statistics in the soft gamma-ray range available for this giant flare. For an optically thin thermal bremsstrahlung spectrum with $kT_{br}=30$ keV we obtain a conversion factor of 1 ACS count s $^{-1}$ $\sim 4.3 \times 10^{-10}$ erg cm $^{-2}$ s $^{-1}$ in the 80-2000 keV energy range.

3. Properties of the 2004 December 27 giant flare

Different distinct features, discussed in the next subsections, are visible in the light curve of the flare shown in Fig. 1, where the original data have been rebinned at 2.5 s: a) a precursor burst¹ 143 s before the flare; b) a short and very intense² initial spike; c) a tail

¹triangulation analysis, using the SPI ACS light curve together with data from other satellites, demonstrates that the arrival direction of this burst is consistent with the position of SGR 1806–20 (Hurley et al. 2005).

²the measured count rate at the peak is $\sim 2 \times 10^6$ counts s $^{-1}$ while the Y-axis scale in Fig. 1 is cut at 1.05×10^5 counts s $^{-1}$

lasting about 400 s, during the first half of which pulsations at the neutron star rotation period are clearly seen.

We have defined $t=0$ at 2004 December 27 21:30:26.55 UT, approximately coinciding with the rise time of the flare. A fit with a constant to the count rate in a 2 ks long time interval before the flare (excluding the precursor) yields a count rate of $\sim 8.8 \times 10^4$ counts s^{-1} , which we use in the following analysis as a constant background level and include it in all the fits keeping its value fixed. Since our data allow to determine the pulsation period with an accuracy of only ~ 0.1 s, we adopt in the following the more precise value of 7.56 s obtained with RXTE (Woods et al. 2005).

3.1. The precursor and the initial spike

The light curve of the precursor binned at full resolution (50 ms) is shown in the inset of Fig. 1. The burst lasted slightly longer than 1 s. It had a rapid rise and decline, and there is some evidence for oscillations over a nearly flat topped profile. For a thermal bremsstrahlung spectrum with $kT_{br}=15$ keV, as estimated with RHESSI (Hurley et al. 2005), the burst fluence of $\sim 9,280$ ACS counts corresponds to 4.4×10^{-6} erg cm^{-2} at $E > 80$ keV. This implies a fluence above 3 keV a factor ten larger than the RHESSI value. A better agreement between the two satellites is obtained for a slightly higher temperature $kT_{br} \sim 20-25$ keV. The phase of the event rise time with respect to the 7.56 s pulsations (see below) is $\phi \sim 0.1$, which does not correspond to those of the peaks seen in the pulsating tail.

The giant flare starts with a short and intense spike during which the ACS count rate remains above 10^6 counts s^{-1} for 0.7 s. The time profile at the peak is strongly affected by dead time and saturation effects which cannot be easily modelled. Therefore the timing analysis of the initial spike and an estimate of its energetics are deferred to a future publication.

3.2. The pulsating tail

The transition from the initial spike to the pulsating tail is displayed at full resolution in Fig. 2. The light curve in the time interval 1.2–2.2 s is well fitted by a power law function $F \propto t^{-\delta}$ with $\delta = 2.1 \pm 0.1$ (as mentioned above a constant fixed at the pre-flare level is included in the fit). A narrow burst, lasting ~ 0.2 s, occurs at $t=2.8$ s, while a broader bump is present in the time range from ~ 2 to 5 s. The latter is in phase ($\phi=0.35-0.6$) with the main peak of the 7.56 s pulsations and can therefore be considered as the first appearance of the

periodicity. Two more bumps occurring after $t=10$ s are also due to the 7.56 s pulsations, which are clearly visible in the tail until $t\sim 300$ s. The average profile of the pulsations is shown in Fig. 3 (phase $\phi=0$ corresponds to $t=0$ s). This has been obtained by folding the data of the time interval 7.56–300 s, i.e. excluding the first pulse which is dominated by the initial spike, at the period of 7.56 s. The pulse profile evolves during the flare with the relative intensity of the second peak increasing with time (Fig. 4).

To characterize the long-term decay profile we have binned the data in time intervals of 7.56 s (see inset of Fig. 2). In this way the short-term variations due to the pulsations are removed. The count rate in the time interval $t\sim 15$ –400 s is well fitted by an exponential function with decay constant $\tau=138\pm 5$ s. Note that the first bin ($t=7.57$ –16.4 s) does not contain the initial hard spike. Nevertheless it lies significantly above the fitted exponential function. Assuming a thermal bremsstrahlung spectrum with $kT_{br}=30$ keV, similar to the tails of the other giant flares, the fluence in the time interval 1–400 s is $\sim 2.6\times 10^{-4}$ erg cm $^{-2}$ for $E>80$ keV (by extrapolation we find a fluence of $\sim 6.4\times 10^{-3}$ erg cm $^{-2}$ for $E>3$ keV).

3.3. Emission after 400 s

The ACS data show evidence for a second, separate component in addition to the main flare discussed above. In fact the count rate increases again at $t\sim 400$ s, forming a long bump which peaks around $t\sim 600$ –800 s and returns to the pre-flare background level at $t\sim 3000$ s (see Fig. 5). Count rate variations on similar timescales are relatively common in the ACS and can be explained by changes in the incident flux of charged particles. Particle-induced background variations are also visible in the counting rate of the Plastic Scintillator Anti-Coincidence (PSAC), a thin (5 mm) detector located just below the SPI coded mask aperture, which is sensitive to charged particles and almost completely transparent to hard X-ray photons. The fact that, contrary to other flux variations, the 400–3000 s ACS bump is not visible in the PSAC light curve (Fig. 5 inset), provides evidence that it is not particle-induced and it is most likely due to SGR 1806–20.

After accounting for the background, estimated from a linear fit to the ACS count rate for $t<0$ s and $t>4000$ s, the time profile decay in the interval $t=500$ –3000 s can be reasonably well described as a power law $F\propto t^{-\delta}$ with $\delta\sim 0.85$. The fluence in the 400–3000 s time interval is approximately equal to that contained in the pulsating tail ($t=1$ –400 s).

4. Discussion

The main features of the December 27 giant flare, i.e. the presence of a very bright short spike and of a decaying tail modulated at the neutron star spin period, are very similar to those of the two giant flares of SGR 0526–66 and SGR 1900+14. There are, however, a few important differences, the most notable of which is the global energetics of the event. The hard X-ray fluence in the SGR 1806–20 initial spike (Hurley et al. 2005; Terasawa et al. 2005) implies an isotropic-equivalent energy release³ of several $10^{46} d_{15}^2$ erg. This is at least two orders of magnitude larger than that of the two other giant flares (1.6×10^{44} erg for SGR 0526–26; $> 7 \times 10^{43}$ erg for SGR 1900+14). The much higher energy involved in the giant flare from SGR 1806–20 is also reflected in the properties of its transient radio emission which reached a luminosity a factor 500 (Cameron et al. 2005, Gaensler et al. 2005) larger than that seen in SGR 1900+14 after the 27 August 1998 event (Frail et al. 1999).

On the other hand, the energy output in the pulsating tail ($1.6 \times 10^{44} d_{15}^2$ erg for $E > 3$ keV) is similar to that of SGR 1900+14 (5×10^{43} erg) and of SGR 0526–66 (4×10^{44} erg). Note that this value does not change significantly for different spectral assumptions and even considering the additional energy output in the emission after $t=400$ s would only double the energy budget. The giant flare of SGR 1806–20 is thus characterized by a much higher spike-to-tail energy ratio ($\gtrsim 100$) than the previous two giant flares (~ 1). According to the magnetar model for giant flares essentially all the energy release occurs during the initial ~ 0.2 s transient phase when a hot relativistic fireball is launched. A fraction of this energy is trapped by closed field lines in the neutron star magnetosphere, forming an optically thick photon-pair plasma which evaporates giving rise to the radiation observed in the pulsating tail (Thompson & Duncan 1995). The magnetic field strength limits the amount of energy that can be confined. The fact that this quantity is similar in the three giant flares, despite the much higher total energy release of SGR 1806–20, is consistent with a magnetic field of the same order in the three magnetars. In fact the pulsating tails of the three giant flares are also similar as far as their durations and timing properties are concerned: their envelopes are reasonably well fitted with exponential laws with decay constants of ~ 70 – 140 s and are modulated by the neutron star rotation with time-variable pulse profiles (Feroci et al. 2001).

The emission after $t \sim 400$ s could originate from the neutron star surface and/or magnetosphere or, alternatively, from the interaction of the relativistic fireball with the surrounding medium. A search for pulsations in the ACS data at times after $t=400$ s gave a negative result, favoring the second interpretation. The afterglow produced by the SGR 1806–20

³we scale our results to a distance of 15 kpc (Corbel & Eikenberry 2004) although recent radio measurements indicate a smaller distance (Cameron et al. 2005)

giant flare has been observed in the radio band (Gaensler et al. 2005; Cameron et al. 2005), yielding estimates of the minimum energy in magnetic field and relativistic particles, E , of several 10^{43} erg (see also Nakar, Piran & Sari 2005). The hard X-ray fluence in the 400-3000 s time interval is consistent with this value. With simple gamma-ray burst afterglow models based on synchrotron emission we can estimate the bulk Lorentz factor Γ from the time t_0 of the afterglow onset: $\Gamma \sim 15 (E / 5 \cdot 10^{43} \text{ erg})^{1/8} (n / 0.1 \text{ cm}^{-3})^{-1/8} (t_0 / 100 \text{ s})^{-3/8}$, where n is the ambient density (see, e.g. Zhang & Meszaros 2003, and references therein). Alternatively, the observed re-brightening could be due to an Inverse Compton component implying a high density environment and a high electron radiation efficiency.

Thanks to the large effective area of the ACS above 100 keV, we can clearly see variations in the pulse profile at high energies. The different evolution of the two emission components visible in the pulsating tail (see Fig. 4) suggests two separate emission regions. It is interesting to note that the pulsations are present since the very early phase of the flare, as indicated by the broad pulse visible at $t=2-4$ s (Fig. 2). This pulse persists at the same rotational phase in the following cycles, while a secondary peak at $\phi \sim 0.75$ gradually emerges. The double-peaked profile is similar to that seen at lower energy with RHESSI (Hurley et al. 2005). We finally note that the short burst at $t=2.8$ s does not appear to be related to other (persistent) structures of the pulsed profile. Its short duration (~ 0.2 s) is typical of the normal soft bursts usually seen from this source and other soft repeaters. This suggests that the mechanisms at the origin of the normal bursts was still operating a few seconds after the giant flare.

We thank K. Hurley, G. Ghisellini and M. Feroci for useful comments. This work has been partially funded by the Italian Space Agency. The SPI-ACS is supported by the German "Ministerium fur Bildung und Forschung" through the DLR grant 50.0G.9503.0.

REFERENCES

- Aptekar R.L., Frederiks D.D., Golenetskii S.V. et al. 2001, ApJSS 137, 227
- Boggs S. et al. 2005, GCN Circ. n. 2936
- Borkowski J., Götz D., Mereghetti S. et al. 2004, GCN Circ. n. 2920
- Cameron P.B. et al. 2005, submitted to Nature, astro-ph/0502428
- Campbell P. et al. 2005, GCN Circ. n. 2932
- Corbel S. & Eikenberry S.S. 2004, A&A 419, 191
- Feroci M. et al. 1999, ApJ 515, L9

Feroci M. et al. 2001, *ApJ* 549, 1021

Frail D.A., Kulkarni, S.R. & Bloom, J.S., 1999, *Nature*, 398, 127

Gaensler, B.M., et al., 2005, submitted to *Nature*, astro-ph/0502393

Gögüş, E., Kouveliotou, C., Woods, P.M., et al. 2001, *ApJ*, 558, 228

Golenetskii S.V., Aptekar R., Mazets E. et al. 2004a, GCN Circular n. 2769

Golenetskii S.V. et al. 2004b, GCN Circular n. 2923

Götz, D., Mereghetti S., Mirabel F.I. & Hurley K. 2004, *A&A* 417, L45

Hurley K., Cline T., Mazets E. et al. 1999, *Nature* 397, 41

Hurley K. et al. 2004, GCN Circular n. 2921

Hurley K. et al. 2005, submitted to *Nature*, astro-ph/0502329

Ibrahim A.I., Swank J.H. & Parke W. 2003, *ApJ* 584, L171

Mazets E.P. et al. 1979, *Nature* 282, 587

Mazets E.P. et al. 2004, GCN Circ. n.2922

Mereghetti S., Götz D., Borkowski J. et al. 2004, GCN Circular n. 2763

Mereghetti S., Götz D., Mirabel I.F & Hurley K. 2005a, *A&A*, in press, astro-ph/0411695

Mereghetti S., Tiengo A., Esposito P. et al. 2005b, submitted to *ApJ*, astro-ph/0502417

Nakar E., Piran T. & Sari R. 2005, astro-ph/0502052

Palmer D. et al. 2004, GCN Circular n. 2925

Smith E. et al. 2005, GCN Circular n. 2927

Terasawa, T. et al., 2005, submitted to *Nature*, astro-ph/0502315

Thompson, C., & Duncan, R.C. 1995, *MNRAS*, 275, 255

von Kienlin A., Beckmann V., Rau A., et al. 2003, *A&A*, 411, L299

Weidenspointner G., Kiener J., Gros M. et al. 2003, *A&A* 411, L113

Woods P.M. & Thompson C. 2004, astro-ph/0406133

Woods P.M., Kouveliotou C., Gögüş E., et al. 2004, *The Astronomer's Telegram*, 313

Woods P.M., Finger M., Patel S. et al. 2005, GCN Circular n. 2950

Zhang B. & Mészáros P. 2003, astro-ph/0311321

Fig. 1.— ACS light curve of the whole flare binned at 2.5 s. The peak of the flare, reaching an observed count rate $\gtrsim 2 \times 10^6$ counts s^{-1} , is not shown. The inset shows the light curve of the precursor burst at full resolution (50 ms).

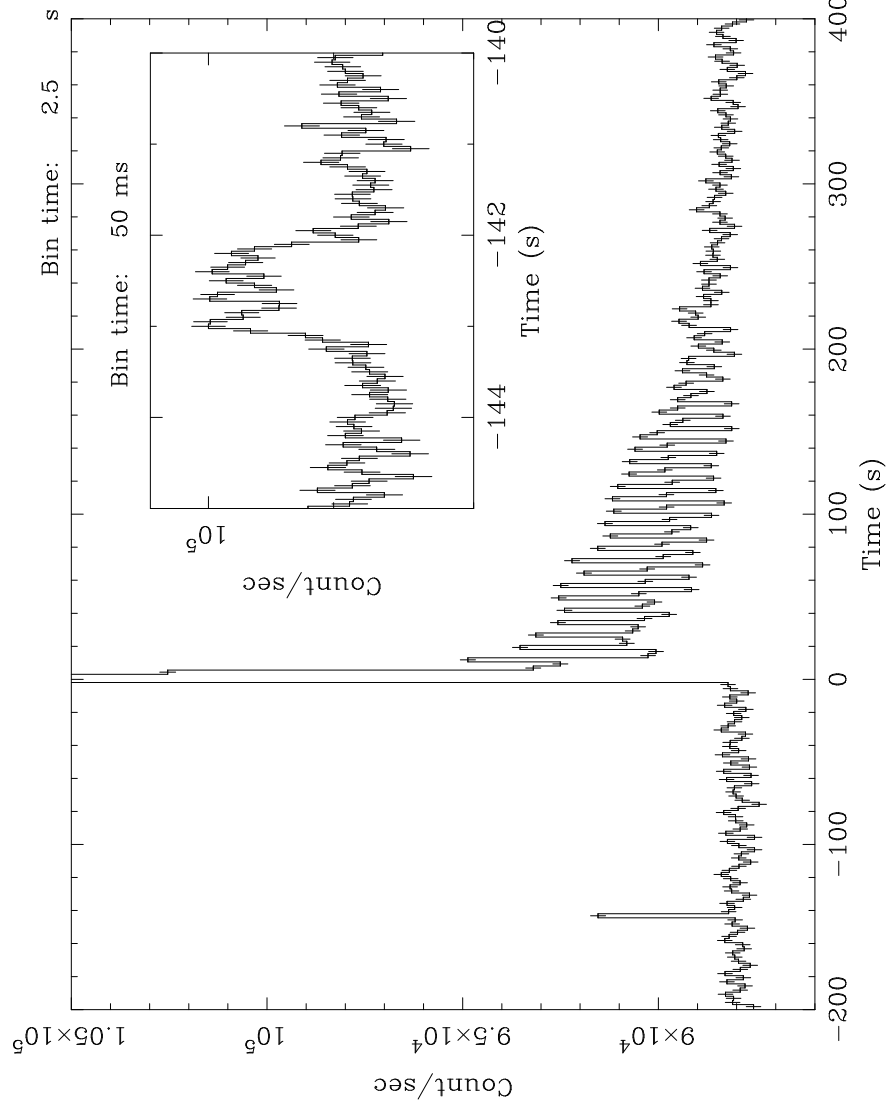


Fig. 2.— Declining part of the initial spike. The line is a fit with a power law plus a constant (fixed at the pre-flare level) to the count rate in the time interval 1.2–2.2 s. The inset shows the light curve of the tail binned at the spin period (7.56 s) and fitted with an exponential function.

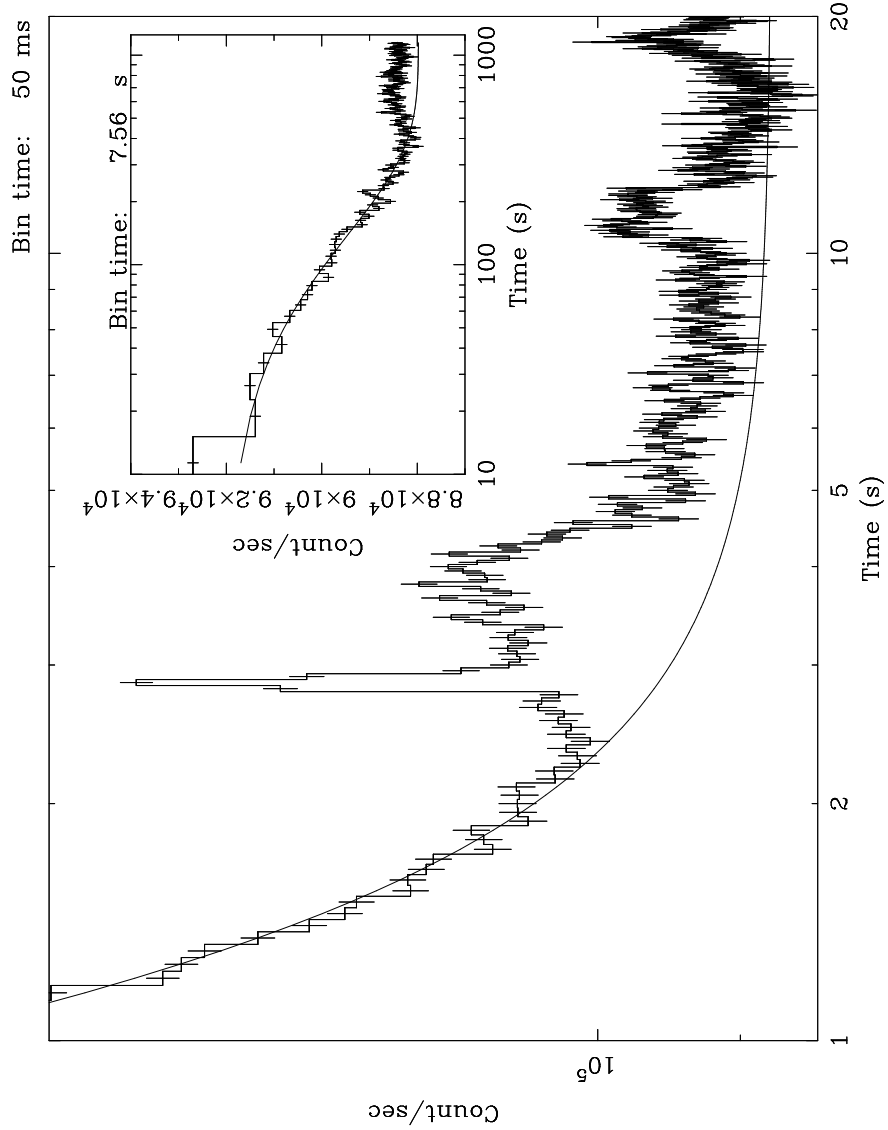


Fig. 3.— Averaged pulse profile obtained by folding the data of the time interval 7.56–300 s.

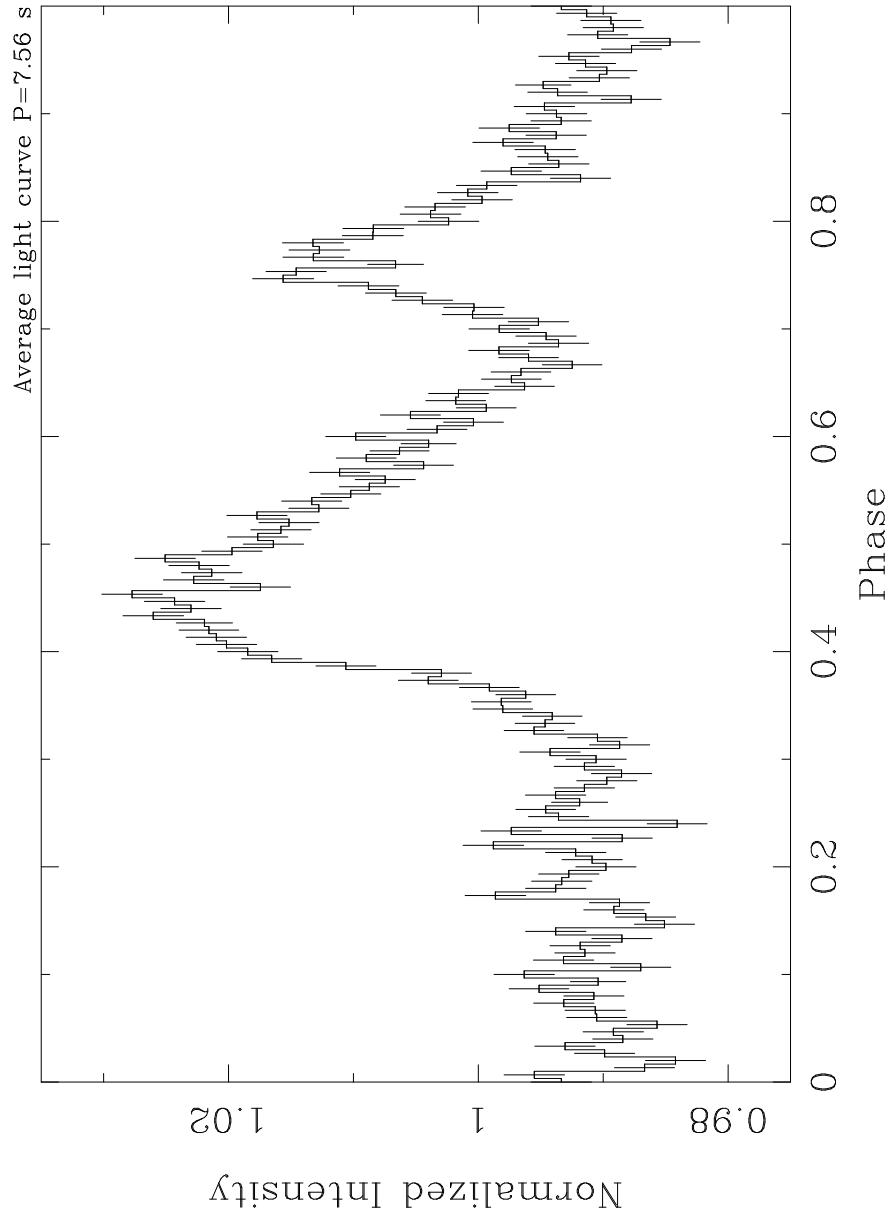


Fig. 4.— Individual light curves of the first 24 pulses. Each panel covers one rotation period of 7.56 s. The top-left panel refers to the time interval 0–7.56 s (the subsequent periods follow from left to right and top to bottom). The X axes give the phase and the Y axes the normalized intensity (except for the first panel where a scale factor has been applied).

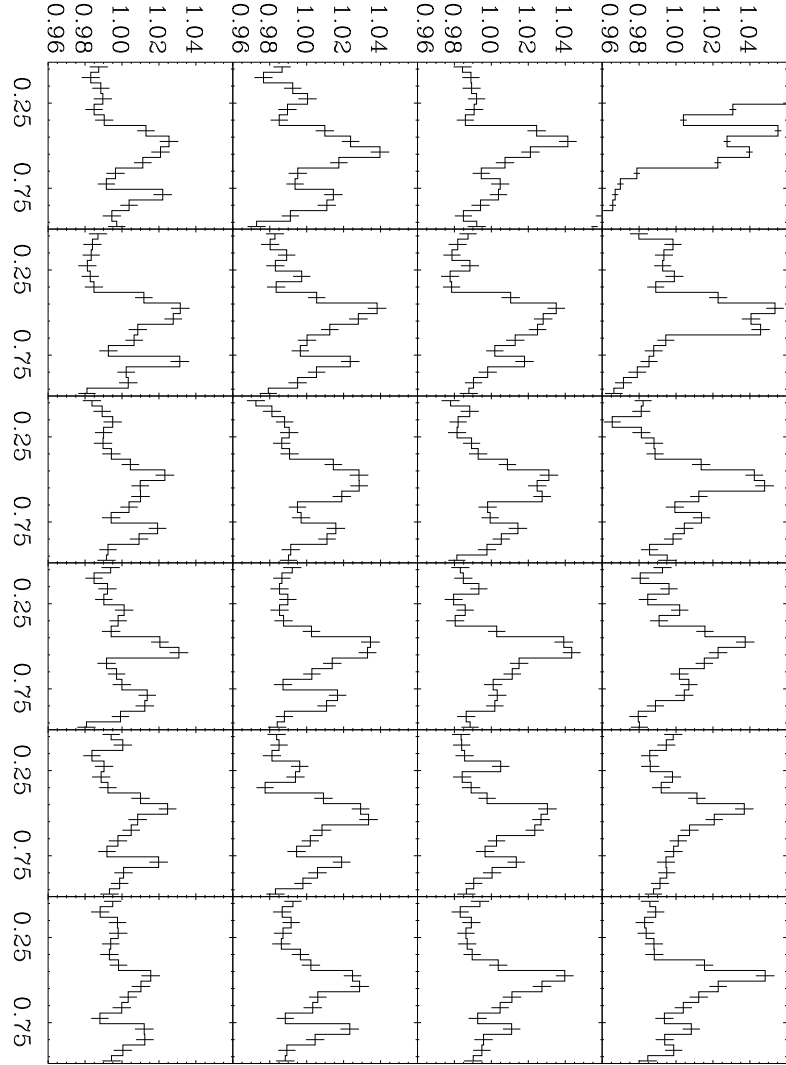


Fig. 5.— SPI ACS light curve of SGR 1806–20 binned at 40 s. The count rate settles back to the pre-flare level after $t \sim 3000$ s. In the inset the ACS (top) and PSAC (bottom) light curves are compared. The extended emission after the giant flare is not visible in the PSAC, while particle induced variations are visible in both detectors.

